Direction-of-Arrival Estimation From a Mixture of Linear and Magnitude-Only Measurements

Weijian Chen, Zai Yang, *Senior Member, IEEE*, and Zhiqiang Wei, *Member, IEEE*

***Abstract*—We address the issue of direction-of-arrival (DOA) estimation by utilizing both linear and magnitude-only (phaseless) measurements. We formulate the DOA estimation problem as an $l_{2,1}$ norm minimization problem by exploiting joint sparsity among the multi-snapshot measurements. We propose an algorithm based on the alternating direction method of multipliers (ADMM) in which both subproblems admit closed-form solutions. The proposed approach does not require any reference signals. Simulation results demonstrate that combining outputs of conventional antennas with magnitude-only antennas significantly improves the accuracy of DOA estimation, and the proposed $l_{2,1}$-ADMM algorithm outperforms the existing methods.**

***Index Terms*—Alternating direction method of multipliers (ADMM), direction-of-arrival (DOA) estimation, magnitude-only measurements, $l_{2,1}$ norm minimization.**

I. Introduction

Direction-of-arrival (DOA) estimation is a crucial problem in array signal processing that involves determining the directions from which an antenna array receives incoming signals. This estimation is vital for various applications, including radar, sonar, wireless communications, and acoustics. Several parametric methods have been proposed to tackle the DOA estimation problem. Among them the most widely used techniques are the Multiple Signal Classification (MUSIC) algorithm [1] and the Estimation of Signal Parameters via Rotational Invariance Technique (ESPRIT) [2]. Additionally, methods based on compressed sensing [3], [4] have been applied to enhance the performance of DOA estimation, particularly in scenarios with limited snapshots or underdetermined systems. These approaches generally provide high-resolution estimates under ideal conditions.

However, in many practical scenarios, phase information required by traditional high-resolution DOA estimation methods may be unreliable due to factors such as sensor calibration errors, noise, or environmental conditions. In some cases, only the magnitude information of the received signals may be accessible. In particular, phase retrieval plays a crucial role in disciplines such as X-ray crystallography, coherent diffraction imaging, optical imaging, and astronomical observations, where the detection systems are typically designed to capture only intensity data [5], [6], [7]. The phase component of the signal is often difficult and costly to measure directly, motivating the need for efficient algorithms that can recover both the amplitude and phase of the underlying signal from magnitude-only measurements. This challenge arises from the inherent ambiguity in phase retrieval, as the magnitude of a complex signal does not uniquely determine its phase, leading to the development of various mathematical and computational techniques aimed at solving this ill-posed inverse problem. To tackle this problem, in [8], the fasT grOup sparsitY Based phAse Retrieval (ToyBar) algorithm, based on the proximal gradient method, is proposed for non-coherent DOA estimation. It resolves inherent ambiguities by incorporating reference signals, similar to the approach in [7]. Additionally, in a different study, the DOA estimation problem with hybrid observations is reformulated as a sparse signal recovery problem, which can be solved using generalized approximate message passing [9]. Nevertheless, this method still relies on the presence of a reference signal.

To address the challenges posed by linear and magnitude-only hybrid observations, we first formulate the DOA estimation problem as an $l_{2,1}$ norm minimization problem, and then we propose an algorithm within the alternating direction method of multipliers (ADMM) framework for joint phase information and DOA estimation. Unlike previous studies [7], [8], [9], which typically rely on at least one reference signal, our method works without any reference signals. This simplification enhances its practical applicability. Experimental results demonstrate the effectiveness of leveraging magnitude-only observations, with the $l_{2,1}$-ADMM algorithm consistently outperforming alternative methods in terms of root-mean-square error (RMSE). These results highlight the algorithm's robustness and its effectiveness in real-world applications, providing significant enhancements in DOA estimation accuracy even under challenging conditions.

The rest of this paper is organized as follows: In Section II, we present the signal model. Section III provides the problem formulation and solution. Then, we present numerical results with discussions in Section IV. Finally, conclusions are draw in Section V.

Notations: Scalars are represented by lower-case letters, while vectors and matrices are denoted by bold lower-case and upper-case letters, respectively. The set of complex numbers is $\mathbb{C}$. $\langle\cdot,\cdot\rangle_{\mathbb{R}}$ denotes the inner product of two matrices. For vector $\boldsymbol{x}$, $\boldsymbol{x}_j$ denotes the j-th element. For matrix $\boldsymbol{A}$, $\mathbb{E}\{\boldsymbol{A}\}$, $\bar{\boldsymbol{A}}$, $\boldsymbol{A}^T$, $\boldsymbol{A}^H$, $\|\boldsymbol{A}\|_F$ and $\boldsymbol{A}^{-1}$ denote the expectation, conjugate, transpose, conjugate transpose, Frobenius norm, and inverse of $\boldsymbol{A}$, respectively. $\mathcal{CN}(\boldsymbol{\mu},\boldsymbol{\Sigma})$ denotes a circularly symmetric complex Gaussian distribution with mean $\boldsymbol{\mu}$ and covariance $\boldsymbol{\Sigma}$. The symbol $\circ$ denotes the Hadamard product, and $\angle$ represents the phase of a complex number.

II. Signal Model

Consider a uniform linear array (ULA) of M omnidirectional sensors with a half-wavelength spacing, and assume a set of K narrowband far-field sources in angular directions $\theta_1,\ldots,\theta_K$, summarized as $\boldsymbol{\theta}=[\theta_1,\ldots,\theta_K]^T$. We assume that the angle remains constant over L time periods. The multi-channel observations are collected in the multiple measurement vector (MMV) matrix $\boldsymbol{Y}\in\mathbb{C}^{M\times L}$, where $[\boldsymbol{Y}]_{m,l}$ denotes the output at sensor m at time instant l. The conventional MMV model is given by

$$\boldsymbol{Y}=\boldsymbol{A}(\boldsymbol{\theta})\boldsymbol{S}+\boldsymbol{N}, \tag{1}$$

where $\boldsymbol{S}\in\mathbb{C}^{K\times L}$ is the source signal matrix, with $[\boldsymbol{S}]_{k,l}$ denoting the signal transmitted by source k at time instant l, and $\boldsymbol{N}\in\mathbb{C}^{M\times L}$

Received 21 January 2025; revised 7 July 2025; accepted 27 August 2025. Date of publication 3 September 2025; date of current version 13 February 2026. This work was supported in part by the National Natural Science Foundation of China under Grant 12371464, in part by the National Key Research and Development Program of China under Grant 2023YFA1008600, and in part by Qin Chuang Yuan High-Level Innovation and Entrepreneurship Talent Program under Grant QCYRCXM-2023-094. The review of this article was coordinated by Dr. Xuesong Cai. *(Corresponding author: Zai Yang.)*

Weijian Chen is with the School of Mathematics and Statistics, Xi'an Jiaotong University, Xi'an 710049, China (e-mail: chenwj0812@stu.xjtu.edu.cn).

Zai Yang and Zhiqiang Wei are with the School of Mathematics and Statistics, Xi'an Jiaotong University, Xi'an 710049, China, also with the Peng Cheng Laboratory, Shenzhen 518055, China, and also with the Pazhou Laboratory (Huangpu), Guangzhou 510555, China (e-mail: yangzai@xjtu.edu.cn; zhiqiang.wei@xjtu.edu.cn).

Digital Object Identifier 10.1109/TVT.2025.3605470

0018-9545 © 2025 IEEE. All rights reserved, including rights for text and data mining, and training of artificial intelligence and similar technologies. Personal use is permitted, but republication/redistribution requires IEEE permission. See https://www.ieee.org/publications/rights/index.html for more information.

Authorized licensed use limited to: Christopher Newport University. Downloaded on February 23,2026 at 17:01:36 UTC from IEEE Xplore. Restrictions apply.

represents circular and spatio-temporal white Gaussian noise with zero mean and variance σ^2. The $M \times K$ array steering matrix $\boldsymbol{A}(\boldsymbol{\theta})$ in (1) is given by

$$\boldsymbol{A}(\boldsymbol{\theta}) = [\boldsymbol{a}(\theta_1), \ldots, \boldsymbol{a}(\theta_K)], \tag{2}$$

where

$$\boldsymbol{a}(\theta_k) = [1, e^{-j\pi \sin\theta_k}, \ldots, e^{-j\pi(M-1)\sin\theta_k}]^T, \tag{3}$$

is the array manifold vector.

When we consider that some of the M antennas only provide magnitude information, the first M_c chains are conventional RF chains that provide complex-valued measurements. The remaining M_m chains are magnitude-only RF chains, which only offer magnitude measurements [9]. This hybrid configuration combines the complex-valued data from the conventional RF chains with the magnitude-only data from the specialized chains. Since the subsequent M_m antennas provide only magnitude information, the magnitude-aided model can be represented as follows

$$\boldsymbol{Z} = \bar{\boldsymbol{P}} \circ \boldsymbol{Y}, \tag{4}$$

where $\boldsymbol{Z}$ is the mixture of linear and magnitude-only measurements. $\boldsymbol{P} = [\boldsymbol{P}_{\mathrm{C}}; \boldsymbol{P}_{\mathrm{M}}] \in \mathbb{C}^{M\times L}$ is a phase matrix, which means that the phase matrix $\boldsymbol{P} \in \mathbb{C}^{M\times L}$ is formed by vertically stacking an $M_c \times L$ all-ones block $\boldsymbol{P}_{\mathrm{C}}$ (corresponding to the fully-digital RF chains that preserve both magnitude and phase) above an $M_m \times L$ block $\boldsymbol{P}_{\mathrm{M}}$ whose entries are unit-modulus scalars $e^{j\phi_{m,l}}$ representing the per-antenna, per-snapshot phase shifts applied to the magnitude-only chains. Substituting (1) into (4), then the received multi-snapshot hybrid observations can be expressed as follows:

$$\boldsymbol{Z} = \bar{\boldsymbol{P}} \circ \boldsymbol{Y} = \bar{\boldsymbol{P}} \circ (\boldsymbol{A}(\boldsymbol{\theta})\boldsymbol{S} + \boldsymbol{N}) = \bar{\boldsymbol{P}} \circ \boldsymbol{A}(\boldsymbol{\theta})\boldsymbol{S} + \boldsymbol{E}, \tag{5}$$

where $\boldsymbol{E} = \bar{\boldsymbol{P}} \circ \boldsymbol{N}$ represents the noise after taking the modulus. It is worth noting that the reference signal is not introduced in model (5). Our goal is to estimate the DOA from the matrix $\boldsymbol{Z}$. However, the nonlinearity of the phase matrix $\boldsymbol{P}_{\mathrm{M}}$ makes the algorithm design particularly challenging.

III. Problem Formulation and Solution

In this section, we aim to recover both the phase information and the source signals by exploiting the sparsity structure inherent in the source signals matrix. First, we formulate the DOA estimation problem as an $l_{2,1}$ norm minimization problem and then address the $l_{2,1}$ norm minimization problem based on the ADMM framework.

A. Problem Formulation

Sparse signal representation and DOA estimation are interconnected, as DOA estimation often reconstructs sparse signals in the angular domain. Typically, the number of signal sources is much smaller than the number of sensors, resulting in angular sparsity. We define a sparse representation of the magnitude-aided model in (5) as

$$\boldsymbol{Z} = \bar{\boldsymbol{P}} \circ \boldsymbol{A}(\bar{\boldsymbol{\theta}})\boldsymbol{X} + \boldsymbol{E}, \tag{6}$$

where $\boldsymbol{X} \in \mathbb{C}^{N\times L}$ denoting a row-sparse signal matrix, and the over-complete dictionary $\boldsymbol{A}(\bar{\boldsymbol{\theta}}) = [\boldsymbol{a}(\bar{\theta}_1), \ldots, \boldsymbol{a}(\bar{\theta}_N)] \in \mathbb{C}^{M\times N}$ is defined in correspondence to (2), where $\bar{\boldsymbol{\theta}} = [\bar{\theta}_1, \ldots, \bar{\theta}_N]^T$ is obtained by sampling the spatial angles at $N \gg K$ points $\bar{\theta}_1, \ldots, \bar{\theta}_N$. For the sake of simplicity, we omit the argument in the remainder of the paper and refer to the dictionary matrix as $\boldsymbol{A} = \boldsymbol{A}(\bar{\boldsymbol{\theta}})$. We assume that the angle grid is sufficiently fine, such that the true angles are contained in (in practice, close to) the angle grid $\bar{\boldsymbol{\theta}}$. We will not consider the impact of mismatches between the true directions $\boldsymbol{\theta}$ and the grid $\bar{\boldsymbol{\theta}}$ in this paper, which has been widely studied (see, e.g., [4]). It is shown in [10], [11] that using a fine enough grid leads to an accurate solution.

We formulate the DOA estimation problem as an $l_{2,1}$ norm minimization problem based on the model in (6). This formulation leverages the inherent structure of the problem, where the row-wise sparsity of the source signals is exploited to effectively recover the DOA [12], [13]. The $l_{2,1}$ norm minimization problem of DOA estimation from a mixture of linear and magnitude-only measurements is given blow

$$\begin{aligned} \min_{\boldsymbol{X},\bar{\boldsymbol{P}}_{\mathrm{M}}} \ & \lambda||\boldsymbol{X}||_{2,1} + \frac{1}{2}||\boldsymbol{Z} - \bar{\boldsymbol{P}} \circ \boldsymbol{A}\boldsymbol{X}||_F^2 \\ \text{s.t.} \ & |\bar{\boldsymbol{P}}_{\mathrm{M}}| = \boldsymbol{1}. \end{aligned} \tag{7}$$

The constraint $|\bar{\boldsymbol{P}}_M| = 1$ enforces that every entry of the phase matrix $\bar{\boldsymbol{P}}_M$ lies on the complex unit circle, i.e. has unit magnitude. In (7), the data fitting $||\boldsymbol{Z} - \bar{\boldsymbol{P}} \circ \boldsymbol{A}\boldsymbol{X}||_F^2$ is performed by means of the Frobenius norm to match the reconstructed measurements $\boldsymbol{A}\boldsymbol{X}$ in the presence of noise. The regularization parameter $\lambda > 0$ admits balancing the data fitting fidelity versus the sparsity level in $\boldsymbol{X}$. Joint sparsity in $\boldsymbol{X}$ is induced by the $l_{2,1}$ mixed-norm, which is defined as

$$||\boldsymbol{X}||_{2,1} = \sum_{n=1}^{N} ||\boldsymbol{x}_n||_2. \tag{8}$$

For a constant modulus matrix $\boldsymbol{P}$, the Frobenius norm remains invariant under element-wise phase shifts. As a result, (7) can be equivalently expressed as the following problem

$$\begin{aligned} \min_{\boldsymbol{X},\boldsymbol{P}_{\mathrm{M}}} \ & \lambda||\boldsymbol{X}||_{2,1} + \frac{1}{2}||\boldsymbol{P} \circ \boldsymbol{Z} - \boldsymbol{A}\boldsymbol{X}||_F^2 \\ \text{s.t.} \ & |\boldsymbol{P}_{\mathrm{M}}| = \boldsymbol{1}. \end{aligned} \tag{9}$$

To overcome the nonlinearity of the constraint $\boldsymbol{P}_{\mathrm{M}}$, we design an algorithm based on ADMM in next subsection. This approach ensures that the nonlinearity in the phase matrix $\boldsymbol{P}_{\mathrm{M}}$ is effectively handled, leading to a more precise solution for DOA estimation.

B. ADMM-Based Algorithm

In this subsection, we propose a method based on the ADMM framework for the problem discussed above and summarize it into an algorithm. ADMM is an effective optimization technique, particularly well-suited for problems with a decomposable structure. Within this framework, the objective function can be decomposed into two sub-problems, each of which can be solved in closed form.

By introducing auxiliary variable $\boldsymbol{V}$, problem (9) is equivalently transformed into the following problem:

$$\begin{aligned} \min_{\{\boldsymbol{V},\boldsymbol{P}_{\mathrm{M}}\},\boldsymbol{X}} \ & \lambda||\boldsymbol{V}||_{2,1} + \frac{1}{2}||\boldsymbol{P} \circ \boldsymbol{Z} - \boldsymbol{A}\boldsymbol{X}||_F^2 \\ \text{s.t.} \ & \boldsymbol{X} - \boldsymbol{V} = \boldsymbol{0}, \\ & |\boldsymbol{P}_{\mathrm{M}}| = \boldsymbol{1}. \end{aligned} \tag{10}$$

The augmented Lagrangian function of problem (10) is defined as

$$\begin{aligned} \mathcal{L}_\rho(\boldsymbol{V},\boldsymbol{X},\boldsymbol{P}_{\mathrm{M}},\boldsymbol{\Lambda}) = \lambda||\boldsymbol{V}||_{2,1} + \frac{1}{2}||\boldsymbol{P} \circ \boldsymbol{Z} - \boldsymbol{A}\boldsymbol{X}||_F^2 \\ + \langle \boldsymbol{\Lambda}, \boldsymbol{X} - \boldsymbol{V}\rangle_{\mathbb{R}} + \frac{\rho}{2}||\boldsymbol{X} - \boldsymbol{V}||_F^2, \end{aligned} \tag{11}$$

where $\boldsymbol{\Lambda}$ and ρ are the Lagrangian multiplier and penalty parameter, respectively.

Authorized licensed use limited to: Christopher Newport University. Downloaded on February 23,2026 at 17:01:36 UTC from IEEE Xplore. Restrictions apply.

For solving (11), the iterative scheme of the ADMM is

$$\{\boldsymbol{V}^{k+1}, \boldsymbol{P}_{\mathrm{M}}^{k+1}\} = \arg\min_{\boldsymbol{V},\boldsymbol{P}_{\mathrm{M}}} \mathcal{L}_\rho(\boldsymbol{V}, \boldsymbol{X}^k, \boldsymbol{P}_{\mathrm{M}}, \boldsymbol{\Lambda}^k)$$
$$\text{s.t. } |\boldsymbol{P}_{\mathrm{M}}| = \boldsymbol{1}, \tag{12}$$
$$\boldsymbol{X}^{k+1} = \arg\min_{\boldsymbol{X}} \mathcal{L}_\rho(\boldsymbol{V}^{k+1}, \boldsymbol{X}, \boldsymbol{P}_{\mathrm{M}}^{k+1}, \boldsymbol{\Lambda}^k) \tag{13}$$
$$\boldsymbol{\Lambda}^{k+1} = \boldsymbol{\Lambda}^k + \rho(\boldsymbol{X}^{k+1} - \boldsymbol{V}^{k+1}). \tag{14}$$

1) Optimize $\boldsymbol{V}^{k+1}$ and $\boldsymbol{P}_{\mathrm{M}}^{k+1}$: It is worth noting that $\boldsymbol{V}$ and $\boldsymbol{P}_{\mathrm{M}}$ are separable, allowing them to be solved individually. Given $\rho > 0$ and $\{\boldsymbol{X}^k, \boldsymbol{\Lambda}^k\}$, the optimization problem with respect to $\boldsymbol{V}$ in (12) can be expressed as follows

$$\boldsymbol{V}^{k+1} = \arg\min_{\boldsymbol{V}} \lambda||\boldsymbol{V}||_{2,1} + \langle \boldsymbol{\Lambda}^k, \boldsymbol{X}^k - \boldsymbol{V}\rangle_{\mathbb{R}} + \frac{\rho}{2}||\boldsymbol{X}^k - \boldsymbol{V}||_F^2$$
$$= \arg\min_{\boldsymbol{V}} \lambda||\boldsymbol{V}||_{2,1} + \frac{\rho}{2}||\boldsymbol{V} - (\boldsymbol{X}^k + \frac{1}{\rho}\boldsymbol{\Lambda}^k)||_F^2. \tag{15}$$

Let $\boldsymbol{U} = \boldsymbol{X}^k + \frac{1}{\rho}\boldsymbol{\Lambda}^k$, then we have

$$\boldsymbol{V}^{k+1} = \arg\min_{\boldsymbol{V}_{1,:},\ldots,\boldsymbol{V}_{N,:}} \sum_{i=1}^{N} (\lambda||\boldsymbol{V}_{i,:}||_2 + \frac{\rho}{2}||\boldsymbol{V}_{i,:} - \boldsymbol{U}_{i,:}||_2^2), \tag{16}$$

which indicates that involved problem (16) can be broken down into N independent subproblems:

$$\min_{\boldsymbol{V}_{i,:}} \lambda||\boldsymbol{V}_{i,:}||_2 + \frac{\rho}{2}||\boldsymbol{V}_{i,:} - \boldsymbol{U}_{i,:}||_2^2, i = 1, \ldots, N. \tag{17}$$

Clearly, the optimal solution $\boldsymbol{V}_{i,:}^*$ can be obtained in the direction $\boldsymbol{U}_{i,:}$, and it has the form of the formula $\boldsymbol{V}_{i,:}^* = b\boldsymbol{U}_{i,:}$ in which $b \geq 0$ is a parameter. Based on the soft-thresholding operator, the above problem has a closed-form solution which can be explicitly expressed as

$$\boldsymbol{V}_{i,:}^* = \left(1 - \frac{\lambda}{\rho||\boldsymbol{U}_{i,:}||_2}\right)_+ \boldsymbol{U}_{i,:}, i = 1, \ldots, N, \tag{18}$$

where $(\cdot)_+ = \max(\cdot, 0)$. Then, $\boldsymbol{V}^{k+1}$ can be formed out of $\boldsymbol{V}_{i,:}^*$. And $\boldsymbol{P}_{\mathrm{M}}^{k+1}$ is update as follows

$$\boldsymbol{P}_{\mathrm{M}}^{k+1} = e^{j(\angle \boldsymbol{A}\boldsymbol{X}^k)_{((M_c+1):\mathrm{end},:)}}, \tag{19}$$

where $\angle\cdot$ represents the phase of some matrix.

2) Optimize $\boldsymbol{X}^{k+1}$: Given $\boldsymbol{V}^{k+1}$, $\boldsymbol{P}_{\mathrm{M}}^{k+1}$ and $\boldsymbol{\Lambda}^k$, we have

$$\boldsymbol{X}^{k+1} = \arg\min_{\boldsymbol{X}} \frac{1}{2}||\boldsymbol{P}^{k+1} \circ \boldsymbol{Z} - \boldsymbol{A}\boldsymbol{X}||_F^2 + \langle \boldsymbol{\Lambda}^k, \boldsymbol{X}\rangle_{\mathbb{R}}$$
$$+ \frac{\rho}{2}||\boldsymbol{X} - \boldsymbol{V}^{k+1}||_F^2. \tag{20}$$

Then taking the derivative with respect to $\boldsymbol{X}$ yields the closed-form solution as follows:

$$\boldsymbol{X}^{k+1} = (\boldsymbol{A}^H\boldsymbol{A} + \rho\boldsymbol{I})^{-1}(\boldsymbol{A}^H(\boldsymbol{Z} \circ \boldsymbol{P}^{k+1}) - \boldsymbol{\Lambda}^k + \rho\boldsymbol{V}^{k+1}). \tag{21}$$

3) Optimize $\boldsymbol{\Lambda}^{k+1}$: When $\boldsymbol{X}^{k+1}$ and $\boldsymbol{V}^{k+1}$ are given, then we have

$$\boldsymbol{\Lambda}^{k+1} = \boldsymbol{\Lambda}^k + \rho(\boldsymbol{X}^{k+1} - \boldsymbol{V}^{k+1}). \tag{22}$$

Algorithm 1: $l_{2,1}$-ADMM Algorithm for Solving (9).

1: **Input**: $\boldsymbol{Z}$ and $\boldsymbol{A}$.
2: **Initialization**: $\boldsymbol{X}^{(0)}$, $\boldsymbol{V}^{(0)}$ and $\boldsymbol{\Lambda}^{(0)}$. Iteration number $i = 0$, prime and dual thresholds ε_p and ε_d. Regularization parameter λ and penalty parameter ρ.
3: Set $\boldsymbol{X}^{(k)} = \boldsymbol{X}^{(0)}$, $\boldsymbol{V}^{(k)} = \boldsymbol{V}^{(0)}$ and $\boldsymbol{\Lambda}^{(k)} = \boldsymbol{\Lambda}^{(0)}$.
Repeat
4: Joint update $\boldsymbol{V}^{k+1}$ and $\boldsymbol{P}_{\mathrm{M}}^{k+1}$ by (19) and (20);
5: Update $\boldsymbol{X}^{k+1}$ by (22);
6: Update $\boldsymbol{\Lambda}^{k+1}$ by (23);
7: **Until** $||\boldsymbol{R}_p^{k+1}||_F^2 \leq \varepsilon_p$ and $||\boldsymbol{R}_d^{k+1}||_F^2 \leq \varepsilon_d$.
Output: $\boldsymbol{X}^\star$.

4) Termination Criteria: The prime and dual residuals are given as

$$\boldsymbol{R}_p^{k+1} = \boldsymbol{X}^{k+1} - \boldsymbol{V}^{k+1} \text{ and } \boldsymbol{R}_d^{k+1} = \rho(\boldsymbol{V}^k - \boldsymbol{V}^{k+1}), \tag{23}$$

respectively. When $||\boldsymbol{R}_p^{k+1}||_F^2 \leq \varepsilon_p$ and $||\boldsymbol{R}_d^{k+1}||_F^2 \leq \varepsilon_d$, the ADMM iteration is terminated. The prime and dual thresholds, ε_p and ε_d, can be constructed by the absolute and relative tolerances ϵ^{abs} and ϵ^{rel}, respectively. The specific method can be found in [14]. Finally, the steps for solving Problem (9) is detailed in Algorithm 1, which we refer to as $l_{2,1}$-ADMM.

Remark 1: Although classical ADMM convergence guarantees hinge on the convexity of each subproblem [14], our inclusion of a unit-modulus projection makes the overall feasible set non-convex and thus eludes formal proofs. Nonetheless, extensive numerical simulations, omitted here for brevity due to the page limits, consistently demonstrate a rapid, monotonic decrease in the objective value. This empirical convergence behavior, which closely mirrors that of convex ADMM, provides strong evidence that our non-convex $l_{2,1}$-ADMM algorithm reliably converges in practical DOA estimation tasks.

IV. Simulations

In this section, simulation results are provided to show the performance of the proposed $l_{2,1}$-ADMM algorithm. First, we compare the performance of the proposed algorithm with different antenna configurations, validating the effectiveness of magnitude-only antennas, which can indeed improve the accuracy of DOA estimation. We then compare the proposed algorithm with ToyBar [8] to demonstrate that accurate signal recovery can be achieved without reference signals. The step size used in ToyBar is set as $1/(2\mu_{\max}(\boldsymbol{A}^H\boldsymbol{A}))$, where $\mu_{\max}$ is the maximum eigenvalue of $\boldsymbol{A}^H\boldsymbol{A}$. The angle range is $[-90^\circ, 90^\circ]$ with a grid step size of 1. The maximum iteration number of ToyBar and ADMM are set as 30000. The regularization and penalty parameters in ADMM are set as $\lambda = \sqrt{M(L + \log M + \sqrt{2L\log M})}\sigma$ [15] and $\rho = M$, respectively. The absolute and relative tolerances ϵ^{abs} and ϵ^{rel} are both set as 10^{-6}. The number of Monte Carlo simulations is set to $T = 50$, and RMSE is defined as:

$$\mathrm{RMSE}(\hat{\theta}) = \sqrt{\frac{1}{KT}\sum_{t=1}^{T}\sum_{k=1}^{K}(\theta_k - \hat{\theta}_k(t))^2}, \tag{24}$$

where $\hat{\theta}_k$ is the estimated DOA.

A. Comparison With Different Antenna Configurations

In this subsection, we compare the performance of the proposed $l_{2,1}$-ADMM algorithm under different antenna configurations to

Authorized licensed use limited to: Christopher Newport University. Downloaded on February 23,2026 at 17:01:36 UTC from IEEE Xplore. Restrictions apply.

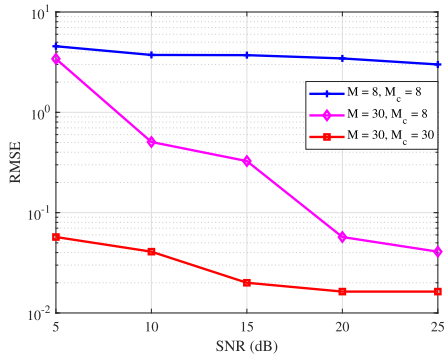

Fig. 1. RMSE versus SNR for different antenna configurations with $L = 50$.

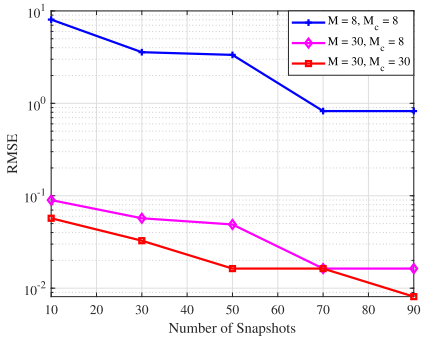

Fig. 2. RMSE versus L for different antenna configurations with SNR $= 20$ dB.

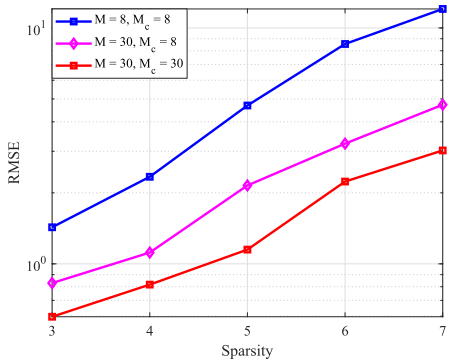

Fig. 3. RMSE versus sparsity for different antenna configuration with $L = 50$ and SNR $= 20$ dB.

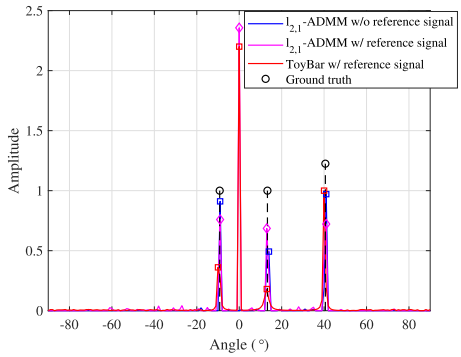

Fig. 4. Spatial spectrum by different methods for $M = 30$, $M_c = 8$, $L = 50$ and SNR $= 20$ dB.

demonstrate that magnitude-only antennas can indeed improve DOA estimation performance. The purpose of this simulation is to systematically assess how array geometry and hardware constraints affect DOA estimation accuracy, and, in particular, to demonstrate that adding low-cost magnitude-only sensors to a limited-RF-chain system can substantially close the performance gap with a fully digital array. We consider three scenarios: first, when $M = M_c = 8$, where the number of antennas is relatively small and the angles cannot be accurately recovered. Second, when $M = M_c = 30$, where the number of antennas is sufficient to accurately recover the angles. Lastly, when $M = 30$, $M_c = 8$, i.e., 22 magnitude-only antennas are introduced to verify the improvement in DOA estimation performance offered by these antennas.

1) RMSE Versus SNR: Fig. 1 illustrates the RMSE of DOA estimation across different SNR levels for three antenna configurations with $L = 50$. In each trial, $K = 3$ sources are uniformly generated within intervals $[-30°, -26°]$, $[15°, 19°]$ and $[23°, 27°]$ respectively. Unless stated otherwise, the method for generating angles used in RMSE comparison remains consistent as described. When $M = M_c = 8$, the RMSE is relatively high due to the limited number of conventional antennas. However, when magnitude-only antennas are introduced, the RMSE decreases more rapidly compared to when $M = M_c = 8$. The configuration with $M = M_c = 30$ consistently delivers the best performance across all SNR levels.

2) RMSE Versus Number of Snapshots: Fig. 2 shows the RMSE of DOA estimation versus the number of snapshots (L) for three antenna configurations with SNR $= 20$ dB. The blue line shows consistently high RMSE, as the limited number of conventional antennas cannot accurately resolve DOA regardless of the number of snapshots. When magnitude-only antennas are introduced, we observe that as the number of snapshots increases, the RMSE for $M = 30$ and $M_c = 8$ gradually decreases. This demonstrates a significant improvement compared to the RMSE for $M = M_c = 8$.

3) RMSE Versus Sparsity: Fig. 3 clearly shows that RMSE increases steadily as the number of sources (K) grows, and that larger or more fully controlled arrays maintain a significant accuracy advantage across the entire range. In particular, the $M = 8$, $M_c = 8$ array exhibits rapidly rising RMSE with each additional path, whereas the $M = 30$, $M_c = 8$ array substantially reduces RMSE across all sparsity levels, narrowing the gap to the large fully digital case. The $M = M_c = 30$ array consistently achieves the lowest RMSE, demonstrating that both aperture size and phase-control capability critically temper the performance degradation induced by increasing sparsity. By combining the results shown in Fig. 1 to Fig. 3, it is evident that magnitude-only antennas play a crucial role in enhancing DOA estimation performance.

B. Comparison With Existing Methods

In this subsection, we compare the $l_{2,1}$-ADMM algorithm with ToyBar to demonstrate its superior DOA estimation performance at same antenna configuration with $M = 30$ and $M_c = 8$. Additionally, since ToyBar requires reference signal, for a fair comparison, we also consider the case where $l_{2,1}$-ADMM includes a reference signal. We consider three DOAs from $-9.2°$, $13.3°$ and $40.6°$ with power vector $[1, 1, 1.5]$ and the reference signal is located at $0°$ and has a power of 9 dB.

1) Spatial Spectrum Versus Existing Methods: Fig. 4 compares the spatial spectrum of various methods with $L = 50$ and SNR $=$ 20 dB. The RMSE of $l_{2,1}$-ADMM algorithm without a reference signal

Authorized licensed use limited to: Christopher Newport University. Downloaded on February 23,2026 at 17:01:36 UTC from IEEE Xplore. Restrictions apply.

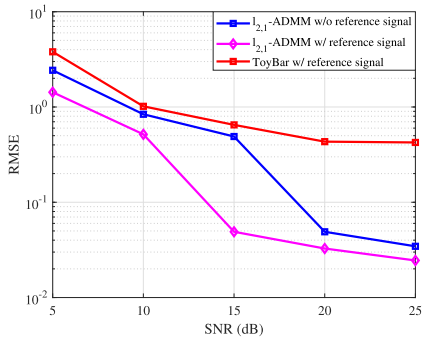

Fig. 5. RMSE versus SNR for different methods with $L = 50$.

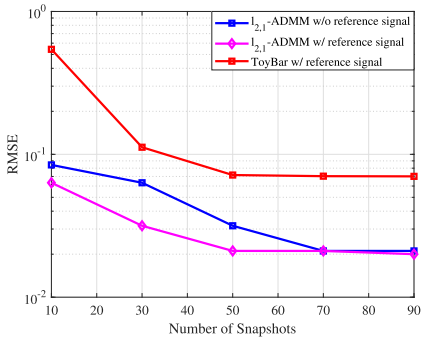

Fig. 6. RMSE versus L for different methods with SNR $= 20$ dB.

is nearly identical to that of the $l_{2,1}$-ADMM algorithm with a reference signal. Furthermore, we can see that the $l_{2,1}$-ADMM algorithm achieves performance similar to that of ToyBar.

2) RMSE Versus SNR: Fig. 5 shows the RMSE of different algorithms as the SNR varies with $L = 50$. The proposed $l_{2,1}$-ADMM algorithm clearly outperforms the ToyBar, regardless of whether a reference signal is used. Furthermore, the $l_{2,1}$-ADMM algorithm with a reference signal performs better than the $l_{2,1}$-ADMM algorithm without it. This enhancement can be attributed to the greater power of the reference signal, which improves the overall SNR of the measurements. More specifically, without a reference signal, the $M \times L$ received matrix satisfies $\boldsymbol{Y} = \boldsymbol{AS} + \boldsymbol{N}, \quad \boldsymbol{N} \sim \mathcal{CN}(0, \sigma^2 \boldsymbol{I})$, so that $\text{SNR}_0 = \mathbb{E}\|\boldsymbol{AS}\|_F^2 / \mathbb{E}\|\boldsymbol{N}\|_F^2$. Injecting a known sequence $\boldsymbol{s}_0 \in \mathbb{C}^{1\times L}$ with amplitude $\boldsymbol{a}_0$ gives $\boldsymbol{Y} = \boldsymbol{AS} + \boldsymbol{a}_0\boldsymbol{s}_0 + \boldsymbol{N}$, and the signal power increases by $|\boldsymbol{a}_0|^2\|\boldsymbol{s}_0\|_2^2$, yielding $\text{SNR}_1 = \frac{\mathbb{E}\|\boldsymbol{AS}\|_F^2 + |\boldsymbol{a}_0|^2\|\boldsymbol{s}_0\|_2^2}{ML\sigma^2} = \text{SNR}_0 + \frac{|\boldsymbol{a}_0|^2\|\boldsymbol{s}_0\|_2^2}{ML\sigma^2} > \text{SNR}_0$.

3) RMSE Versus Number of Snapshots: Fig. 6 shows the RMSE of various algorithms as the number of snapshots (L) varies with SNR $= 20$ dB. As the number of snapshots increases, the RMSE decreases for all methods. Furthermore, the $l_{2,1}$-ADMM algorithm outperforms ToyBar, regardless of whether a reference signal is included. Notably, the $l_{2,1}$-ADMM with a reference signal demonstrates the best performance, achieving the lowest RMSE even with fewer snapshots. By combining Fig. 4 to Fig. 6, we can see that the proposed $l_{2,1}$-ADMM algorithm outperforms the existing methods, validating the superior performance of our method.

V. Conclusion

This correspondence first formulated the DOA estimation problem as an $l_{2,1}$-norm minimization problem in hybrid observation models that include both linear and magnitude-only measurements, and then proposed an $l_{2,1}$-ADMM algorithm for jointly estimating phase information and DOA without the need for reference signals. Experimental results highlight the effectiveness of magnitude-only antennas in improving estimation accuracy, with the proposed algorithm outperforming previous methods like ToyBar.

References

[1] P. Stoica and A. Nehorai, "MUSIC, maximum likelihood, and Cramer–Rao bound," *IEEE Trans. Acoust., Speech, Signal Process.*, vol. 37, no. 5, pp. 720–741, May 1989.
[2] R. Roy and T. Kailath, "ESPRIT-estimation of signal parameters via rotational invariance techniques," *IEEE Trans. Acoust., Speech, Signal Process.*, vol. 37, no. 7, pp. 984–995, Jul. 1989.
[3] Z. Yang and L. Xie, "Exact joint sparse frequency recovery via optimization methods," *IEEE Trans. Signal Process.*, vol. 64, no. 19, pp. 5145–5157, Oct. 2016.
[4] Z. Yang, J. Li, P. Stoica, and L. Xie, "Sparse methods for direction-of-arrival estimation," in *Academic Press Library in Signal Processing*, vol. 7 New York, NY, USA: Elsevier, 2018, pp. 509–581.
[5] E. J. Candes, Y. C. Eldar, T. Strohmer, and V. Voroninski, "Phase retrieval via matrix completion," *SIAM Rev.*, vol. 57, no. 2, pp. 225–251, Feb. 2015.
[6] Y. Shechtman, A. Beck, and Y. C. Eldar, "GESPAR: Efficient phase retrieval of sparse signals," *IEEE Trans. Signal Process.*, vol. 62, no. 4, pp. 928–938, Feb. 2014.
[7] H. Kim, A. M. Haimovich, and Y. C. Eldar, "Non-coherent direction of arrival estimation from magnitude-only measurements," *IEEE Signal Process. Lett.*, vol. 22, no. 7, pp. 925–929, Jul. 2015.
[8] Z. Wan and W. Liu, "A fast group sparsity based phase retrieval algorithm for non-coherent DOA estimation," in *Proc. 54th Asilomar Conf. Signals, Syst., Comput.*, Jun. 2021, pp. 220–224.
[9] S. Wang, K. Nie, M. He, and Y. He, "DOA estimation aided by magnitude measurements," *IEEE Trans. Veh. Technol.*, vol. 70, no. 11, pp. 12197–12202, Nov. 2021.
[10] G. Tang, B. N. Bhaskar, and B. Recht, "Sparse recovery over continuous dictionaries-just discretize," in *Proc. 2013 Asilomar Conf. Signals, Syst. Comput.*, 2013, pp. 1043–1047.
[11] V. Duval and G. Peyré, "Sparse spikes super-resolution on thin grids II: The continuous basis pursuit," *Inverse Problems*, vol. 33, no. 9, 2017, Art. no. 095008.
[12] C. Steffens, M. Pesavento, and M. E. Pfetsch, "A compact formulation for the $l_{2,1}$ mixed-norm minimization problem," *IEEE Trans. Signal Process.*, vol. 66, no. 6, pp. 1483–1497, Mar. 2018.
[13] Y. Jin and B. D. Rao, "Support recovery of sparse signals in the presence of multiple measurement vectors," *IEEE Trans. Inf. Theory*, vol. 59, no. 5, pp. 3139–3157, May 2013.
[14] S. Boyd, N. Parikh, E. Chu, B. Peleato, and J. Eckstein, "Distributed optimization and statistical learning via the alternating direction method of multipliers," *Found. Trends Mach. Learn.*, vol. 3, no. 1, pp. 1–122, 2011.
[15] Y. Li and Y. Chi, "Off-the-grid line spectrum denoising and estimation with multiple measurement vectors," *IEEE Trans. Signal Process.*, vol. 64, no. 5, pp. 1257–1269, Mar. 2016.

Authorized licensed use limited to: Christopher Newport University. Downloaded on February 23,2026 at 17:01:36 UTC from IEEE Xplore. Restrictions apply.